Bioelectrochemistry 88 (2012) 15–21

Contents lists available at SciVerse ScienceDirect

Bioelectrochemistry

journal homepage: www.elsevier.com/locate/bioelechem

Electrochemical impedance spectroscopy characterization of nanoporous alumina dengue virus biosensor

Binh Thi Thanh Nguyen [a], Alister En Kai Peh [a], Celine Yue Ling Chee [a], Katja Fink [b], Vincent T.K. Chow [c], Mary M.L. Ng [c], Chee-Seng Toh [a,*]

[a] Division of Chemistry and Biological Chemistry, School of Physical and Mathematical Sciences, Nanyang Technological University, Singapore 637371, Singapore
[b] Singapore Immunology Network, Agency for Science, Technology and Research, Singapore
[c] Department of Microbiology, Yong Loo Lin School of Medicine, National University of Singapore, Singapore

ARTICLE INFO

Article history:
Received 7 January 2012
Received in revised form 12 April 2012
Accepted 24 April 2012
Available online 2 May 2012

Keywords:
Dengue
Virus
Nanoporous membrane
Diagnostics
Sensor

ABSTRACT

The Faradaic electrochemical impedance technique is employed to characterize the impedance change of a nanoporous alumina biosensor in response towards the specific binding of dengue serotype 2 (Denv2) viral particles to its serotype 2-specific immunoglobulin G antibody within the thin alumina layer. The optimal equivalent circuit model that matches the impedimetric responses of the sensor describes three distinct regions: the electrolyte solution (R_s), the porous alumina channels (including biomaterials) (Q_1, R_1) and the conductive electrode substrate layer (Q_2, R_2). Both channel resistance R_1 and capacitance Q_1 change in response to the increase of the Denv2 virus concentration. A linear relationship between R_1 and Denv2 concentration from 1 to 900 plaque forming unit per mL (pfu mL^{-1}) can be derived using Langmuir–Freundlich isotherm model. At 1 pfu mL^{-1} Denv2 concentration, R_1 can be distinguished from that of the cell culture control sample. Moreover, Q_1 doubles when Denv2 is added but remains unchanged in the presence of two other non-specific viruses — West Nile virus and Chikungunya virus indicates biosensor specificity can be quantitatively measured using channel capacitance.

1. Introduction

Nanobiosensors have developed rapidly in recent years, among which thin film-coated and membrane-based nanobiosensors are highly promising owing to rapid analysis time, excellent analytical performance, simple fabrication and analysis procedures. Nanoporous thin film based on alumina have been used for the electrochemical detection of penicillin [1], and proteins [2] including glucose oxidase [3] and West Nile virus [4]. In addition, these nanoporous films and membranes when coupled to cyclic voltammetry, differential pulse voltammetry or electrochemical impedance spectroscopy (EIS) methods are highly useful for DNA hybridization detection [5,6] and bacteria sensing [7]. Generally, these detection methods rely on the interaction of the target species at the electrode/electrolyte interface or within the nanoporous channels of the alumina layer.

Comparatively, electrochemical impedance spectroscopy has been a more useful tool to investigate the physico-chemical characteristics of the electrode/electrolyte interface. Unlike the other electroanalytical methods, EIS probes a wide frequency range hence reaction rates to identify processes including electron transfer, chemical reaction, species absorption, electrolyte conductance and mass transport of redox probe [8,9]. Until now, impedance behaviours of alumina porous layers have been well studied using EIS which were initially described using a simple RC circuit of the porous layers [10–12]. Subsequently, the capacitance was replaced by the constant phase element (CPE) because of non-homogenity of the porous layer giving rise to distribution of capacitance values [13].

Diagnoses of viral diseases are usually performed using immunoassay methods including ELISA (enzyme-linked immunosorbent assay) where the analyte targets are antibodies raised in response to the viruses in the infected patient. Direct detection of viruses is highly desired and has been recently achieved by viral capture methods using antibody immobilized alumina membrane-based biosensor [4]. Herein, EIS is used to investigate the changes of the electrode/electrolyte interface impedance when the nanoporous alumina membrane is immobilized with immunoglobulin G (IgG) antibody and virus to provide a basic understanding for current and potentially increasingly widespread virus sensing applications using the nanoporous membrane-based biosensors. Dengue virus is chosen as the model analyte in this work because of its widespread occurrence with an estimated 50 million cases of dengue fever cases, and ca. 22,000 deaths worldwide per year [14]. Rapid and accurate diagnosis of dengue infection is therefore essential for timely and appropriate treatment besides control of the disease. Herein, dengue serotype 2 (Denv2) is chosen as the model analyte as it is one of the most frequently observed serotypes in Singapore and its surrounding region.

* Corresponding author. Tel.: +65 65922553; fax: +65 67911961.
E-mail address: cstoh@ntu.edu.sg (C-S. Toh).

1567-5394/$ – see front matter © 2012 Elsevier B.V. All rights reserved.
doi:10.1016/j.bioelechem.2012.04.006

2. Materials and methods

2.1. Reagents and materials

Anti dengue serotype 2 antibody, (clone 3H5, isotype IgG, 1.0 mg mL^{-1}) was purchased from Millipore. Bovine Serum Albumin (BSA, >98%), ferrocenemethanol (FeMeOH, >99%) and phosphate buffered saline (PBS, 10×), were purchased from Sigma Aldrich. Phosphoric acid (85%) was purchased from Lancaster Synthesis. All chemicals and solvents were of analytical grade and used as received. Ultrapure water (Sartorius Ultrapure Water System) was used for all preparations.

2.2. Virus cultivation and inactivation

Aedes mosquito cells (C6/36) were infected with dengue serotype 2 viruses at a Multiplicity of Infection (MOI) of 0.01 for 1 h at 28 °C. Following this, the medium was removed and fresh growth medium (RPMI, 5% heat-inactivated fetal bovine serum (FBS) and 5 mM 2-mercaptoethanol) was added. After which, the cell culture was incubated at the same temperature for 5 days. After 5 days, the medium was collected and a plaque assay was carried out to determine the concentration of the dengue virus in terms of plaque forming unit (pfu mL^{-1}). The dengue virus sample was subsequently heat-inactivated at 56 °C for 30 min.

2.3. Preparation of nanobiosensor

The preparation procedure of the nanoporous alumina electrode follows previous report [3]. Home-made nanoporous alumina electrodes were fabricated using platinum wires embedded in epoxy sheaths and micropipette tips. The electrode tip was polished with 1.0 μm and 0.3 μm diameter alumina powder before sputter-coated with aluminium metal film. Sub-micrometer thick aluminum films in the thickness range of 300–500 nm were sputter-coated onto the platinum electrodes using 99.999% purity aluminum target, Denton discovery® 18 Sputtering System and sputtering power of 100 W in an atmosphere of research-grade Ar at 5×10^{-3} Torr. Anodization of aluminum coated electrodes were conducted using previously described method of pipette contact anodization method. This was carried out by positioning a glass pipette coated with ca. 40 nm thick platinum layer, above and in contact with the surface of the aluminum coated electrode. 0.1 M oxalic acid solution was then added into interior portion of the platinum coated glass pipette. The aluminum coated layer was anodized potentiostatically in the 0.1 M oxalic acid at 40 V versus the platinum counter electrode placed in the glass pipette. To prepare the nanobiosensor, the nanoporous alumina electrode was first etched in 3% phosphoric acid for 15 min and washed thoroughly with copious amount of PBS (Fig. 1). Solutions of 3H5 antibody, BSA and dengue virus solutions were prepared in PBS. BSA was used as blocking agent for non-specific binding sites. Immobilization of the respective reagents was subsequently carried out by spreading 5 μl of the reagent solution across the alumina electrode surface. The antibody was immobilized for 1 h followed by BSA while virus capture was carried out with 30 min incubation time. After each immobilization step, the alumina electrode was rinsed extensively with PBS and then characterized using cyclic voltammetry.

2.4. Characterization of the nanobiosensor

All electrochemical measurements were carried out on an autolab potentiostat/galvanostat (Eco Chemmie, Netherland) using a three electrode cell containing the nanoporous alumina electrode as working electrode, a silver/silver chloride reference electrode and a platinum wire counter electrode in PBS pH 7.4 solution containing 1 mM ferrocenemethanol. Cyclic voltammetry was carried out at a potential range from −0.2 to 0.6 V with a scan rate of 0.05 V s^{-1}. Impedance measurements were performed over the frequency range from 0.1 Hz to 100 kHz at the mid-peak potential of ferrocenemethanol derived from cyclic voltammetry (~0.19 V versus Ag/ACl, 1 M KCl) with alternating current potential amplitude of 50 mV. The impedance data was fitted to an equivalent circuit model using the EIS spectrum analyzer programme. The fitting quality was evaluated by chi-squared (R^2) value and error percentage corresponding to each component of the equivalent circuit model.

3. Result and discussion

3.1. Characterization using cyclic voltammetry

Fig. 2 shows the typical cyclic voltammograms of the alumina electrode after each step of the nanobiosensor preparation procedure: before and after chemical etching, antibody immobilization, BSA immobilization and virus capture in PBS (pH = 7.4) containing 1 mM ferrocenemethanol redox probe. It is observed that the current transmission of the alumina electrode is increased by etching. This is attributed to the further widening of the alumina nanopores (or nanochannels) with phosphoric acid thus allows more redox probe to enter the nanochannel and increases the Faradaic current [3,4,15,16]. The magnitude of the current decreases further after each of the following antibody, BSA immobilization and virus capture steps, due to enhanced barriers either at the electrode–electrolyte interface and/or the thin alumina layer. Though the peak height decreases, the anodic and cathodic peak positions are unchanged after the several immobilization steps which strongly suggest that the loading of antibodies and subsequent virus capture do not influence the charge transfer kinetics significantly at the electrode–electrolyte region [17]. It is also observed that there is a gradual decrease in the current with increasing amount of the dengue virus added, consistent with other analyte targets using nanoporous membrane biosensors [4,15]. Presumably, this decrease in current is related to the amount of the immunocomplexes formed within the nanochannels so ought to provide a close correlation between the signal change and virus concentration using an equilibrium binding theory.

3.2. Characterization using the electrochemical impedance spectroscopy

Herein, EIS is used to investigate the processes that occur within the nanoporous thin alumina coated biosensor which is highly relevant to understand several recent biosensing works involving thin film and membrane-based biosensors for viruses, living cells and other biological species [2,4,7,15,18–20]. Unlike cyclic voltammetry and differential pulse voltammetry which derive mass transfer limited signal responses at high overpotentials, EIS data are derived at near equilibrium conditions close to the formal potential of the redox probe. Thus, EIS can probe other physical processes that occur during the virus capture events within the nanoporous structure of the thin alumina layer of the biosensor, and possibly construct an alternative method for direct virus detection in contrast to the mass transfer limiting approach [4,15,21].

Fig. 3A,B shows the real and imaginary parts of the impedance of the nanobiosensor with respect to frequency in the presence of increasing virus concentrations from 1 to 900 pfu mL^{-1}. The real and imaginary parts of the impedance is calculated from the overall impedance (Z^*): $Z^*(\omega) = Z'(\omega) + jZ''(\omega)$ where ω is the angular frequency and equals $2\pi f$ (f/Hz is the frequency). It is shown that at frequencies lower than 1 Hz, both the real impedance Z' and imaginary impedance Z'' are increased after exposure to the viral particles. At the lowest frequency, the change in the overall impedance Z^* at 1 pfu mL^{-1} virus concentration is ~10 times larger than that of a solution containing cell culture medium in the absence of virus. Clearly, the biosensor presents sensitive response towards the presence of immobilized proteins and viral particles in the low frequency range.

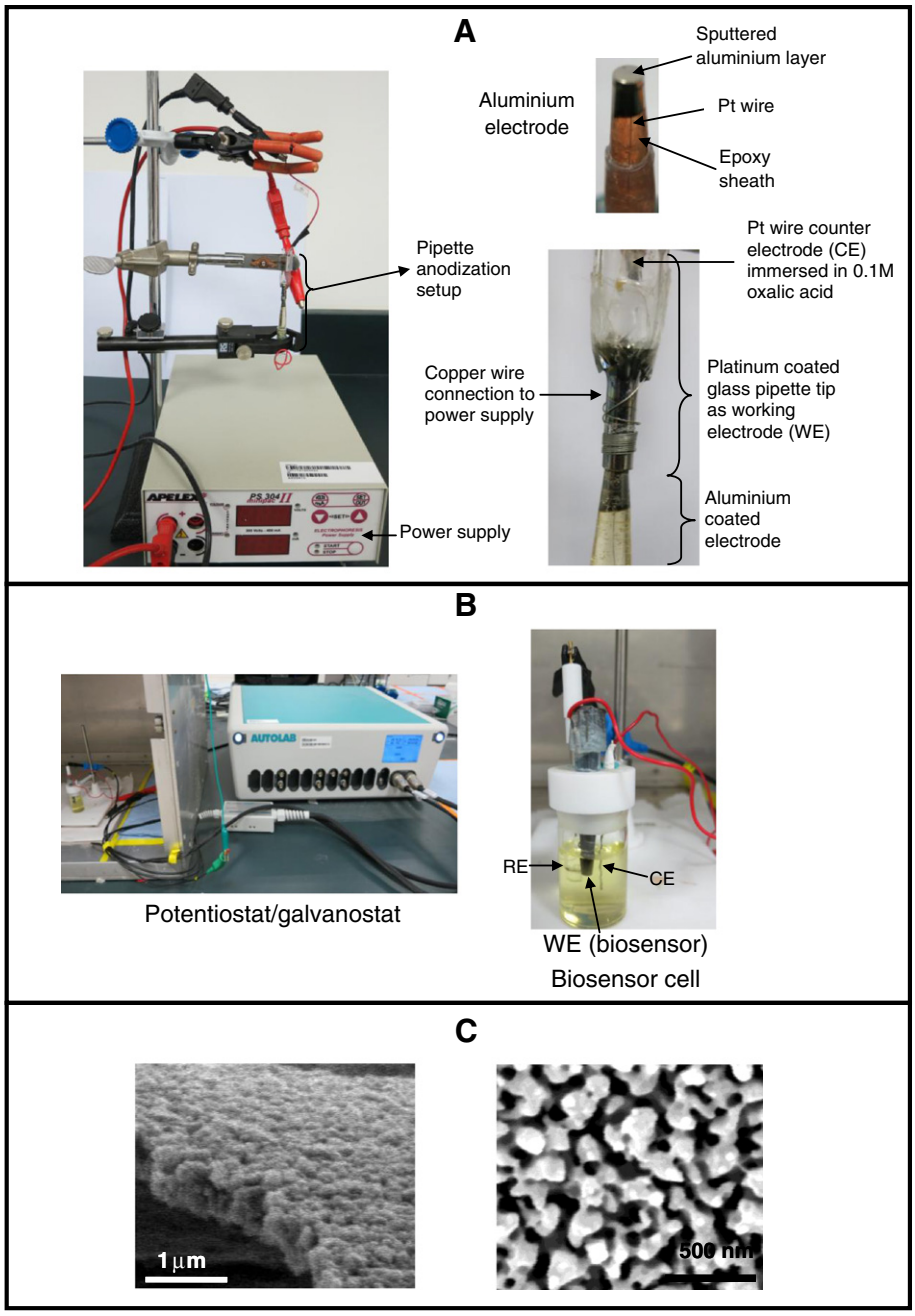

Fig. 1. (A) Anodization setup for the preparation of alumina electrode. (B) EIS setup for the characterization of the virus biosensor. (C) Scanning electron micrographs of an unetched nanoporous alumina electrode and its alumina surface after 15 min etching in 3% phosphoric acid.

In contrast, at higher frequencies, all the traces overlapped which indicates the curves do not depend on the presence of virus particles, and are thus not useful for virus detection. This differential change in Z^* at increasing virus concentration is clearly indicated by the enlarging traces of the Nyquist plot (Fig. 3C). No straight line tails are observed at low frequency range indicates the absence of a Warburg probe diffusion-controlled process [22]. This indicates diffusion of the redox probe is not rate-limiting under the conditions of the impedance measurements, unlike voltammetric measurements [4,15].

Interestingly, two maxima in the Bode-phase plot well separated in the frequency domain are observed for the etched alumina electrode (Fig. 3D), which clearly indicates two time constants. Since the physical structure of the alumina electrode comprises the nanochannel-solution and the electrode–solution interfaces, the interactions of virus particles can change the impedimetric responses of these two interfaces. Thus the time constant at high frequency range is attributed to the faster charge transfer at the conductive electrode-solution interface while the low frequency region presents the movement of ions along the nanochannels [23]. The phase shift of the first maximum at ca. 14 Hz increases with immobilization of the antibody probe and subsequent addition of the virus particles. In contrast, the second maximum at ca. 400 Hz decreases significantly upon immobilization of the antibody probe and a less obvious change when more virus particles are added to the solution.

The optimal model that matches the impedimetric responses of the thin nanoporous alumina biosensor comprises a series of two constant phase elements in parallel with two resistances, which is consistent with an insulating porous layer on top of a conductive layer (Fig. 4). Three distinct regions can be identified: the electrolyte solution (R_s), the porous alumina channels (including proteins and viral particles)

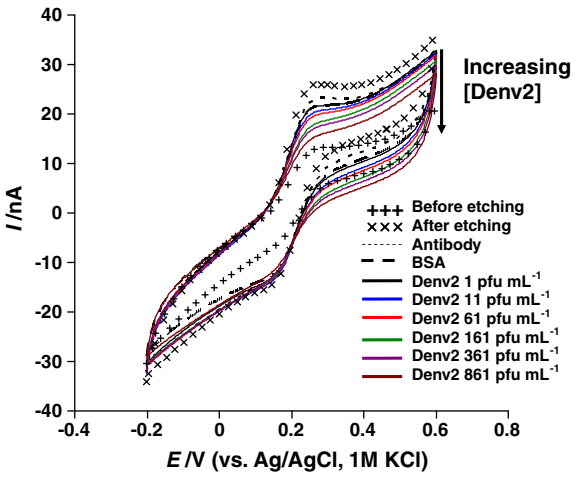

Fig. 2. Cyclic voltammetry of the alumina electrode after each step of the nanobiosensor preparation procedure: before and after chemical etching, antibody immobilization, BSA immobilization and virus capture in PBS (pH = 7.4) containing 1 mM ferrocenemethanol redox probe.

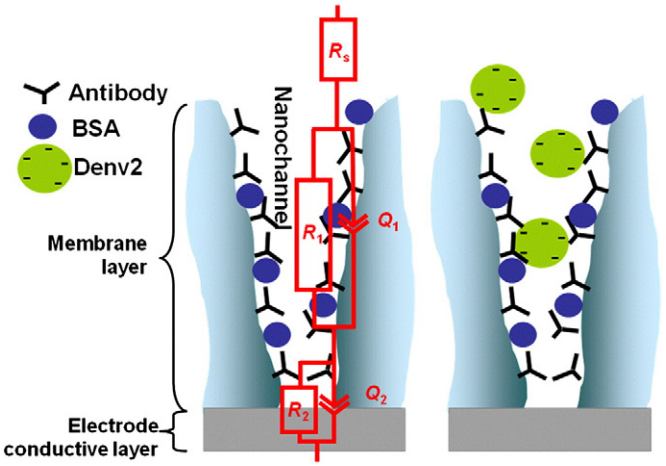

Fig. 4. Schematics of the porous alumina nanobiosensor for Denv2 virus detection by specific binding to immunoglobulin G antibody 3H5 positioned along the walls of the alumina nanochannels. The equivalent circuit model is inserted.

(CPE_1, R_1) and the conductive electrode substrate layer (CPE_2, R_2). The constant phase element (CPE) was used to describe the non-Faradaic process at the alumina-solution and electrode-solution layers, in contrast to the capacitance element to take into account of the topological imperfection of the alumina porous layer and the conductive electrode layer. This is in agreement with previous works on porous structures such as thin nanoporous alumina membrane which has been modeled using non-Faradaic components comprising a channel resistance in parallel with a constant phase element which represents the channel capacitance [10,13,24,25]. The impedance of CPE is given as both the parameter Q and the exponent n and it is defined as $Z_{CPE} = 1/(Q(j\omega)^n)$, $Q/n\Omega^{-1}s^n$ is an adjustable parameter used in the non-linear least square fitting routine is the angular frequency; when the value of the exponent n is equal to 1, the CPE acts as a pure capacitor.

Table 1 shows the values of the circuit elements obtained by fitting the experiment data in Fig. 3 and two other repeated experiments.

Table 1 shows that the fitted R_1 and R_2 parameters. R_1 and R_2 are attributed to channel resistance and slow charge transfer kinetics respectively at the alumina electrode. From the fitted impedance values of R_1 in Table 1, we estimate the channel resistivity, $\rho_c = 420(\pm 21)$ MΩ cm using the relation $R_1 = \rho_c l_c / A_c$ between ρ_c/Ω cm, channel length l_c (~300 nm), channel cross-section area A_c and channel resistance, R_1. This resistivity value is similar to the channel resistivity of a 60 μm thick alumina membrane placed in a solution of similar ionic strength [10,26]. We observe an increase in the channel resistance R_1 responses in the presence of increasing virus concentration

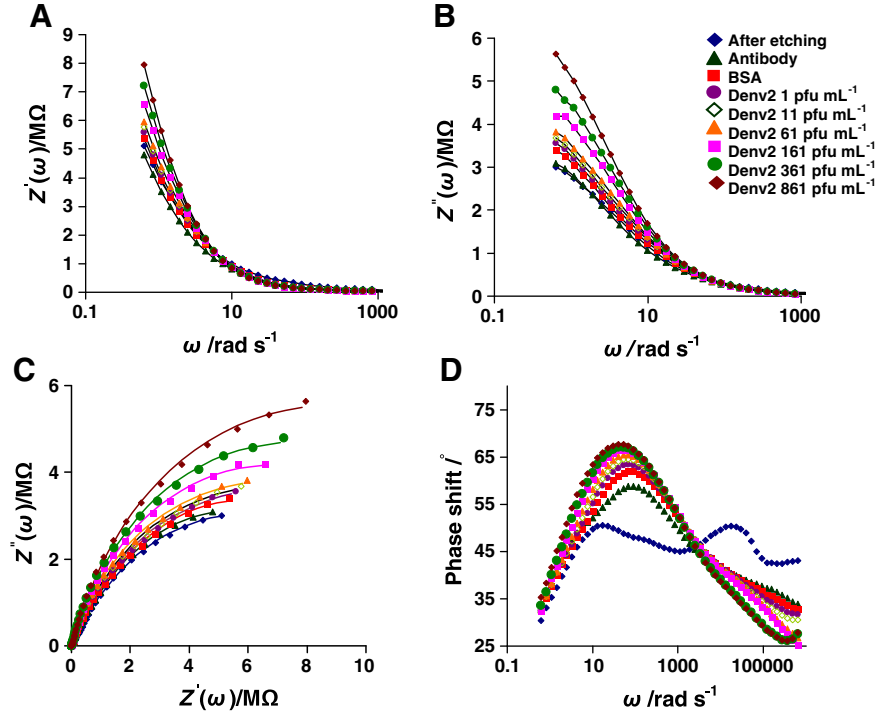

Fig. 3. (A) Real (in-phase) impedance Z', (B) imaginary (out-of-phase) impedance Z'' versus angular frequencyω, (C) Nyquist plot and (D) Bode-phase plot of the biosensor after Denv2 virus capture from solutions of increasing virus concentration. Measurements were conducted in PBS (pH = 7.4) containing 1 mM ferrocenemethanol.

Table 1
Fitted EIS results of the nanobiosensor using the equivalent circuit shown in Fig. 3 and an average bulk solution resistance $R_s = 1.9$ kΩ.

	R_1[a]/kΩ	R_2[b]/MΩ	Q_1[a]/μΩ^{-1} s^n	n_1	Q_2[b]/μΩ^{-1} s^n	n_2
BSA/Ab	16.91 ± 0.89	9.08 ± 0.43	0.46 ± 0.07	0.51 ± 0.02	0.12 ± 0.004	0.72 ± 0.001
Denv2 1 pfu mL^{-1}	18.26 ± 1.18	9.08 ± 0.47	0.57 ± 0.09	0.50 ± 0.02	0.12 ± 0.005	0.73 ± 0.003
Denv2 11 pfu mL^{-1}	20.10 ± 1.35	9.24 ± 0.39	0.65 ± 0.11	0.49 ± 0.02	0.11 ± 0.004	0.75 ± 0.003
Denv2 61 pfu mL^{-1}	22.50 ± 1.73	9.62 ± 0.38	0.69 ± 0.12	0.48 ± 0.02	0.10 ± 0.004	0.76 ± 0.003
Denv2 161 pfu mL^{-1}	26.00 ± 1.74	10.84 ± 0.36	0.67 ± 0.11	0.49 ± 0.02	0.10 ± 0.003	0.78 ± 0.003
Denv2 361 pfu mL^{-1}	30.43 ± 0.71	11.57 ± 0.53	0.95 ± 0.02	0.44 ± 0.00	0.09 ± 0.003	0.79 ± 0.004
Denv2 861 pfu mL^{-1}	34.61 ± 0.89	13.46 ± 0.74	1.08 ± 0.02	0.43 ± 0.00	0.09 ± 0.003	0.79 ± 0.004

[a] R_1 and Q_1 are channel resistance and capacitance respectively at the nanochannel region.
[b] R_2 and Q_2 are charge transfer resistance and capacitance respectively at the electrode–electrolyte region.

which is attributed to either channel blocking by non-specific proteins or by specific viral particles. The immobilization of these biomolecules along nanochannel can reduce the channel area thus causes the increase in channel resistance.

Conversely, the heterogeneous rate constant for ferrocenemethanol Faradaic reaction can be described using the following relation between the heterogeneous rate constant k_{ct}, concentration of redox species C, electrode area A and the change in charge transfer resistance R_2 (Eq. (1)):

$$R_2 = RT/\left(n^2F^2k_{ct}AC\right) \tag{1}$$

where R is the gas constant, T is the temperature, n is number of electrons transferred and F is the Faraday constant.

In the presence of increasing virus concentration, the charge transfer resistance R_2 increases (Table 1). Similar to R_1, this could occur due to specific binding of virus or non-specific physical adsorption of proteins and cells fragments at the electrode–electrolyte interface which can reduce the electrode area, causing increase in the charge transfer resistance. From an average R_2 value of 10 MΩ, it is estimated that the heterogeneous rate coefficient $k_{ct} = 0.66(\pm 0.03) \times 10^{-3}$ cm s^{-1} which agrees closely with previous values determined from voltammetric peak-to-peak distance [17] .

Interestingly, the channel capacitance Q_1 changes significantly in the presence of virus, for example, 100% increase is observed from 1 to 900 pfu mL^{-1} virus concentration. Similar effects on surface capacitance of alumina have been observed due to binding of charged species [27]. In this case, the capture of negatively charged viral particles with pI of 5 in pH 7.4 PBS solution, to the antibody-coated alumina nanochannel walls, is the most likely cause of this increase in channel capacitance. In contrast, the change in electrode–electrolyte capacitance Q_2 is only ca. 20% when the Denv2 concentration is changed from 1 to 900 pfu mL^{-1}. The significant change in the value of n_1 further corroborates with binding of virus particles or other species within the channels, since any deviation of n_1 from 1 represents a non-smooth surface. In comparison, the n_2 values are closer to 1 than those of n_1 as expected for the more homogeneous metal electrode surface compared to the antibody-coated nanochannel walls.

3.3. Denv2-antibody binding affinity

The specific binding interaction between Denv2 and its antibody is as follows:

$$\begin{aligned} &\mathrm{Ab} + \mathrm{Denv2} \rightleftharpoons \mathrm{Denv2-Ab} \\ &K/\mathrm{M}^{-1} = [\mathrm{Denv2-Ab}]/([\mathrm{Ab}][\mathrm{Denv2}]) \end{aligned} \tag{2}$$

where K/M^{-1} is the affinity constant which describes the strength of the antigen–antibody interaction.

The binding of viral particles within the nanochannels can be described using a simple Langmuir model in which the antibody–antigen binding site is equivalent to an active surface site [4]. Using IgG antibody as the virus capture agent, we found that the Langmuir–Freundlich isotherm was more suitable to explain the relation between sensor signal response and virus concentration [21]. This is attributed to the capture of virus along a nanochannel which creates the largest change in channel resistance compared to subsequent virus capture within the same nanochannel. This is similar to the Langmuir–Freundlich model where the most favourable surface binding occurs first gives the largest change in surface fractional coverage f compared to subsequent surface bindings.

$$f = \frac{KC^{\frac{1}{n}}}{1 + KC^{\frac{1}{n}}} \tag{3}$$

where fractional coverage $f = (R_{\mathrm{Denv2}} - R_{\mathrm{Denv2=0}})/(R_{\mathrm{Denv2max}} - R_{\mathrm{Denv2=0}})$, while n is in the range of 1 to 5, K is the antibody-virus binding constant and C/M is Denv2 concentration.

Non-linear curve-fitted results using Eq. (3) are plotted together with the experimental data derived in Fig. 3 which shows excellent fitting result (Fig. 5A). Rearrangement of Eq. (3) to the logarithm

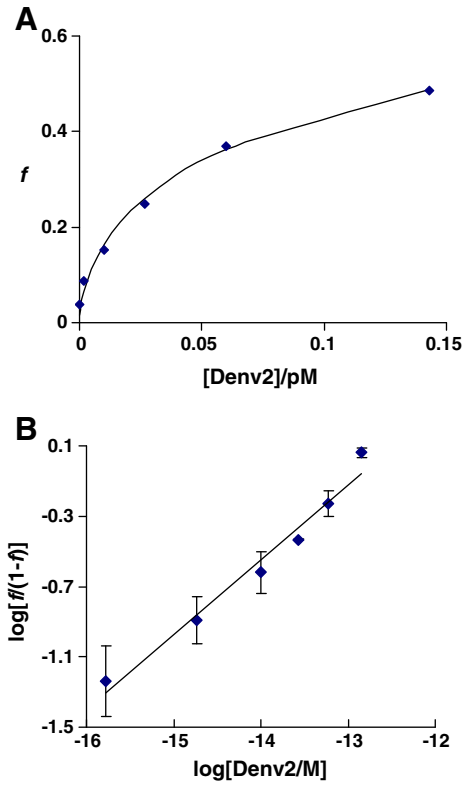

Fig. 5. (A) Plot of fractional coverage f derived from the fitted R_1 values of the nanobiosensor impedimetric response toward Denv2 in PBS (pH = 7.4) and 1 mM ferrocenemethanol, together with the curve-fitted data derived using Eq. (3). (B) Plot of the logarithm of $f/(1-f)$ against the logarithm of Denv2 concentration derived from two different nanobiosensors.

Table 2
Fitted EIS results of the nanobiosensor placed in each of the following solutions: virus-free culture medium (Control), CHK, WNV and Denv2 respectively, in consecutive steps, using the equivalent circuit presented in Fig. 3. Error values are average values derived from three EIS measurements using the same nanobiosensor.

	R_1[c]/kΩ	R_2[d]/kΩ	Q_1[c]/nΩ^{-1} s^n	Q_2[d]/nΩ^{-1} s^n
Control	43.0 ± 1.1	191.2 ± 2.0	39.7 ± 3.2	79.8 ± 1.1
CHK	45.1 ± 1.6	199.9 ± 7.5	48.2 ± 6.6	83.9 ± 2.1
WNV	43.0 ± 0.7	213.4 ± 3.6	44.6 ± 3.3	89.2 ± 2.8
Denv2	47.8 ± 1.8	228.7 ± 0.5	114.8 ± 23.7	90.0 ± 2.9

[c] R_1 and Q_1 are channel resistance and capacitance respectively at the nanochannel region.
[d] R_2 and Q_2 are charge transfer resistance and capacitance respectively at the electrode–electrolyte region.

expression (Eq. (4)) allows the data to be plotted in the linear form (Fig. 5B).

$$\mathrm{Log}\left(\frac{f}{1-f}\right) = \mathrm{Log}\left(K/M^{-1}\right) + \frac{1}{n}\mathrm{Log}(C/M) \quad (4)$$

Interestingly, the calculated binding affinity K from non-linear curve fitting is $4.87 \times 10^7\ M^{-1}$ which is somewhat on the lower range than the reported binding constant of Denv2-IgG (10^9–$10^7\ M^{-1}$) [28] using a reported pfu-to-virus particle ratio of 1:100,000. We attribute this to the difference in the binding affinity of IgG which range from 10- to 10^3-fold decrease when its binding configuration changes from two-arms to one-arm binding [29]. This could arise due to the limited space within the nanochannel.

3.4. Selectivity experiment

To utilize the nanobiosensor in dengue virus diagnosis using impedance measurements, the biosensor has to demonstrate selective responses against other viruses. Table 2 shows the response of a nanobiosensor towards consecutive exposure to non-flavivirus Chikungunya (CHK), flavivirus West Nile virus (WNV), followed by Denv2 which is also member of the flavivirus family. All virus concentrations are 100 pfu mL^{-1} and incubation procedure for virus capture followed by impedance measurement is identical for all three viruses and the control solution. Control solution is the supernatant of the cell culture medium after cell cultivation.

Using the Student's t-test with a p value cutoff of 0.05, the p-analysis indicates the channel capacitance Q_1 is selective for Denv2 over CHK and WNV since p-values are <0.05: Denv2 and CHK ($p = 0.009$); Denv2 and WNV ($p = 0.007$), but cannot differentiate between CHK and WNV: CHK and WNV ($p = 0.44$). In contrast, p-analysis for the other three parameters indicates no clear trend in selectivity. The p-values for channel resistance R_1, charge transfer resistance R_2 and electrode–electrolyte capacitance Q_2 are as follows: Denv2 and CHK (R_1: $p = 0.14$; R_2: $p = 0.003$; Q_2: $p = 0.043$); Denv2 and WNV (R_1: $p = 0.014$; R_2: $p = 0.002$; Q_2: $p = 0.74$); CHK and WNV (R_1: $p = 0.107$; R_2: $p = 0.047$; Q_2: $p = 0.060$).

Clearly, the selectivity for Denv2 is most evident for channel capacitance Q_1 (Table 2) where the channel capacitance Q_1 is unchanged in the presence of WNV and CHK but doubles when Denv2 was added. This suggests that the Denv2 particle interacts specifically with the antibody 3H5 along the nanochannels, unlike the other two viruses. However, the channel resistance R_1 is also responsive to non-specific viruses, which we attribute to blocking of nanochannels by the large viruses at narrower part of the nanochannels, which will limit the mass transfer of the redox probe throughout the entire length of the blocked nanochannels. The pore size distribution of the alumina layer has been previously shown to be largest at the exterior (~70–120 nm) and smallest at the interior part (10–30 nm) close to the electrode-alumina interface [16]. Since the size of virus particles (~50 nm) are in general larger than the smaller non-specific proteins and cell fragments, and therefore, unable to access the electrode surface covered with smaller diameter nanochannels compared to the exterior part of the alumina layer. Thus it is reasonable to conclude that changes in the charge transfer resistance R_2 and capacitance Q_2 of the electrode-solution region are due to non-specific binding at the electrode surface by these smaller proteins and cell fragments present in the virus solution.

These observations appear dissimilar to most other works which measure impedimetric changes of surface bound species. We attribute this apparent discrepancy to the additional alumina overlayer of the membrane-based nanobiosensor which captures most of the specific virus particles before these can reach the electrode-solution interface. Whereas, the non-specific viruses and other constituents of the virus solution can reach the underlying electrode-solution interface and thus influence R_2 and Q_2.

Overall, this proposed specific binding mechanism of Denv2 virus within the nanochannels is consistent with our recent works using other electroanalytical methods that indicate specific response of the nanobiosensor towards dengue compared to other flavi- and non-flaviviruses [21].

4. Conclusions

We have characterized the nanoporous alumina dengue virus biosensor using EIS and a circuit model comprising two R-CPE units arranged in series to delineate the responses of the channel wall-solution component from the electrode-solution interface. Fitted results of the pore resistance R_1 can be correlated to Denv2 concentrations using the Freundlich–Langmuir. In addition, the fitted pore capacitance Q_1 data allows specific identification of Denv2 from two other mosquito-borne viruses (WNV and CHK). These results indicate pore resistance and capacitance are highly useful for quantitative and specific detection of Denv2 in contrast to the electrode/solution capacitance and charge transfer resistance. Significantly, the fitting circuit model ought to be applicable in general to other biosensors utilizing antibody-loaded thin films to capture analyte targets. The capacitance changes within the nanochannels upon specific virus-antibody binding further suggests that monitoring of capacitive signals could be useful for the development of high specificity biosensors.

Acknowledgements

The authors thank the Singapore Immunology Network-Agency for Science, Technology and Research (SIgN-A*STAR) for the research grant (SIgN09-023), Kelly Lau (NUS Microbiology) for her help in dengue virus propagation and plaque assay; and AEKP acknowledge MOE-NUS for the PhD scholarship.

References

[1] P. Takhistov, Electrochemical synthesis and impedance characterization of nano-patterned biosensor substrate, Biosens. Bioelectron. 19 (2004) 1445–1456.
[2] A. De La Escosura-Muñiz, A. Merkoçi, A nanochannel/nanoparticle-based filtering and sensing platform for direct detection of a cancer biomarker in blood, Small 7 (2011) 675–682.
[3] G. Koh, S. Agarwal, P.S. Cheow, C.S. Toh, Development of a membrane-based electrochemical immunosensor, Electrochim. Acta 53 (2007) 803–810.
[4] B.T.T. Nguyen, G. Koh, H.S. Lim, A.J.S. Chua, M.M.L. Ng, C.S. Toh, Membrane-based electrochemical nanobiosensor for the detection of virus, Anal. Chem. 81 (2009) 7226–7234.
[5] S.J. Li, J. Li, K. Wang, C. Wang, J.J. Xu, H.Y. Chen, X.H. Xia, Q. Huo, A nanochannel array-based electrochemical device for quantitative label-free DNA analysis, ACS Nano 4 (2010) 6417–6424.
[6] K.C. Lin, V. Kunduru, M. Bothara, K. Rege, S. Prasad, B.L. Ramakrishna, Biogenic nanoporous silica-based sensor for enhanced electrochemical detection of cardiovascular biomarkers proteins, Biosens. Bioelectron. 25 (2010) 2336–2342.
[7] F. Tan, P.H.M. Leung, Z.B. Liu, Y. Zhang, L.D. Xiao, W.W. Ye, X. Zhang, L. Yi, M. Yang, A PDMS microfluidic impedance immunosensor for *E. coli* O157:H7 and *Staphylococcus aureus* detection via antibody-immobilized nanoporous membrane, Sens. Actuator B Chem. 159 (2011) 328–335.

[8] A.M. Oliveira-Brett, L.A. Silva, G. Farace, P. Vadgama, C.M.A. Brett, Voltammetric and impedance studies of inosine-5′-monophosphate and hypoxanthine, Bioelectrochemistry 59 (2003) 49–56.
[9] C.M.A. Brett, Electroanalytical techniques for the future: the challenges of miniaturization and of real-time measurements, Electroanalysis 11 (1999) 1013–1016.
[10] J. Hitzig, K. Jüttner, W.J. Lorenz, W. Paatsch, AC-impedance measurements on porous aluminium oxide films, Corros. Sci. 24 (1984) 945–952.
[11] J. Hitzig, K. Juettner, W.J. Lorenz, AC-Impedance measurements on corroded porous aluminum oxide films, J. Electrochem. Soc. 133 (1986) 887–892.
[12] B. Van der Linden, H. Terryn, J. Vereecken, Investigation of anodic aluminium oxide layers by electrochemical impedance spectroscopy, J. Appl. Electrochem. 20 (1990) 798–803.
[13] A. Girginov, A. Popova, I. Kanazirski, A. Zahariev, Characterization of complex anodic alumina films by electrochemical impedance spectroscopy, Thin Solid Films 515 (2006) 1548–1551.
[14] D.J. Gubler, Dengue and dengue hemorrhagic fever, Clin. Microbiol. Rev. 11 (1998) 480–496.
[15] M.S. Cheng, S.H. Lau, V.T. Chow, C.S. Toh, Membrane-based electrochemical nanobiosensor for *Escherichia coli* detection and analysis of cells viability, Environ. Sci. Technol. 45 (2011) 6453–6459.
[16] G. Koh, S. Agarwal, P.S. Cheow, C.S. Toh, Characterization of the barrier layer of nanoporous alumina films prepared using surface contact anodization technique, Electrochim. Acta 52 (2007) 2815–2821.
[17] A.J. Bard, L.R. Faulkner, Electrochemical methods: fundamentals and applications, 2nd ed. John Wiley, New York, 2001.
[18] K. Healy, B. Schiedt, I.P. Morrison, Solid-state nanopore technologies for nanopore-based DNA analysis, Nanomedicine 2 (2007) 875–897.
[19] A. Heilmann, N. Teuscher, A. Kiesow, D. Janasek, U. Spohn, Nanoporous aluminum oxide as a novel support material for enzyme biosensors, J. Nanosci. Nanotechnol. 3 (2003) 375–379.
[20] Z. Yang, S. Si, C. Zhang, Study on the activity and stability of urease immobilized onto nanoporous alumina membranes, Microporous Mesoporous Mater. 111 (2008) 359–366.
[21] M.S. Cheng, J.S. Ho, C.H. Tan, J.P.S. Wong, L.C. Ng, C.-S. Toh, Development of an electrochemical membrane-based nanobiosensor for ultrasensitive detection of dengue virus, Anal. Chim. Acta (2012), http://dx.doi.org/10.1016/j.aca.2012.03.017.
[22] T.L. Lasseter, W. Cai, R.J. Hamers, Frequency-dependent electrical detection of protein binding events, Analyst 129 (2004) 3–8.
[23] M.I. Prodromidis, Impedimetric immunosensors—a review, Electrochim. Acta 55 (2010) 4227–4233.
[24] W. Römer, C. Steinem, Impedance analysis and single-channel recordings on nano-black lipid membranes based on porous alumina, Biophys. J. 86 (2004) 955–965.
[25] G. Sharma, M.V. Pishko, C.A. Grimes, Fabrication of metallic nanowire arrays by electrodeposition into nanoporous alumina membranes: effect of barrier layer, J. Mater. Sci. 42 (2007) 4738–4744.
[26] J.A. González, V. López, A. Bautista, E. Otero, X.R. Nóvoa, Characterization of porous aluminium oxide films from a.c. impedance measurements, J. Appl. Electrochem. 29 (1999) 229–238.
[27] O.K. Varghese, D. Gong, M. Paulose, K.G. Ong, C.A. Grimes, E.C. Dickey, Highly ordered nanoporous alumina films: effect of pore size and uniformity on sensing performance, J. Mater. Res. 17 (2002) 1162–1171.
[28] J.S. Schieffelin, J.M. Costin, C.O. Nicholson, N.M. Orgeron, K.A. Fontaine, S. Isern, S.F. Michael, J.E. Robinson, Neutralizing and non-neutralizing monoclonal antibodies against dengue virus e protein derived from a naturally infected patient, Virol. J. 7 (2010).
[29] I. Roitt, J. Brostoff, D. Male, Immunology, 6th ed. Mosby, New York, 2001.